Volume 7 | Number 42 | 14 November 2019 | Pages 6461–6646

Journal of Materials Chemistry B

Materials for biology and medicine

rsc.li/materials-b

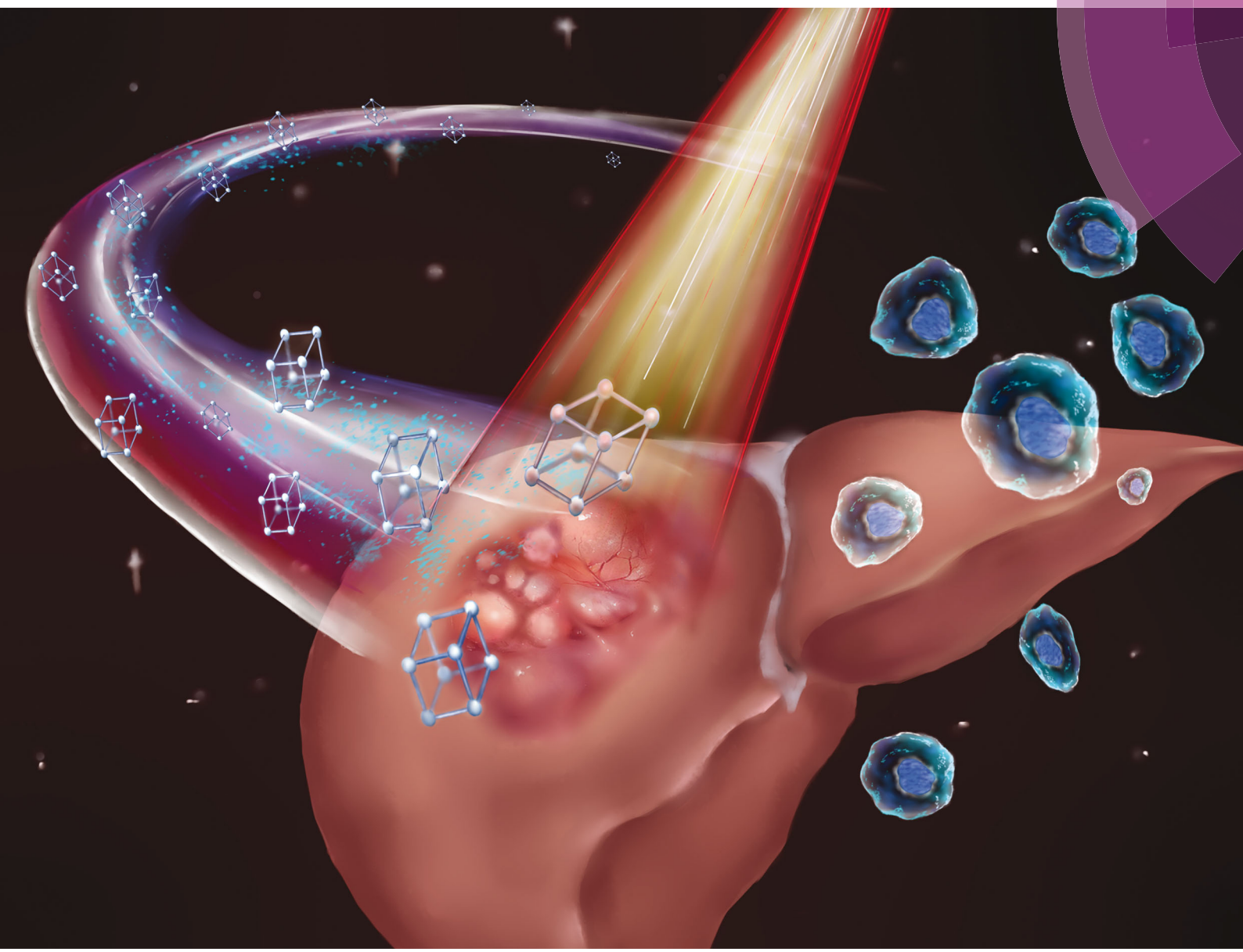

ISSN 2050-750X

ROYAL SOCIETY OF CHEMISTRY | Celebrating IYPT 2019

PAPER

Guocan Yu, Zhengwei Mao, Shusen Zheng *et al.* Combinatorial photochemotherapy on liver cancer stem cells with organoplatinum(II) metallacage-based nanoparticles

Journal of Materials Chemistry B

PAPER

View Article Online
View Journal | View Issue

Published on 29 August 2019. Downloaded by Queen Mary, University of London on 3/3/2022 3:14:37 PM.

Check for updates

Cite this: *J. Mater. Chem. B*, 2019, 7, 6476

Combinatorial photochemotherapy on liver cancer stem cells with organoplatinum(II) metallacage-based nanoparticles†

Beng Yang,‡[a] Hua Liu,‡[a] Huang Yang,[b] Wei Chen,[c] Jingban Wu,[a] Xiaode Feng,[a] Rongliang Tong,[a] Hanxi Yu,[a] Yunhao Chen,[a] Zhen Lv,[a] Weijian Sun,[d] Bin He,[a] Jian Wu,[a] Guocan Yu,*[e] Zhengwei Mao *[b] and Shusen Zheng*[a]

Received 27th June 2019,
Accepted 14th August 2019

DOI: 10.1039/c9tb01299k

rsc.li/materials-b

Liver cancer is a kind of lethal and aggressive malignant neoplasm with a high rate of relapse and metastasis after therapy. An important cause for the relapse and metastasis is the existence of liver cancer stem cells (CSCs), which have high resistance to chemotherapy and high tumorigenic potential. Therefore, it is crucial to develop new methods to eradicate CSCs in tumors. Herein, we develop a photodynamic therapy (PDT) that features bimodal metallacage-loaded nanoparticles (MNPs) for integrated chemotherapy. This platform achieves chemo-photodynamic combinational therapy. Organoplatinum(II) metallacage-loaded nanoparticles show excellent ability to kill liver CSCs, decreasing their mobility and sphenoid formation ability under near-infrared laser irradiation. Importantly, MNPs can successfully penetrate into 3D tumor spheroids, which display higher drug resistance compared to traditional 2D cultured cells. This destroys CSCs and prevents subsequent tumor formation *in vivo*. With the excellent combinational therapeutic results in hand, the working mechanisms of MNPs were then studied. MNPs under NIR light irradiation can generate reactive oxygen species (ROS), resulting in damage of mitochondrial membrane and subsequent cell apoptosis with chemotherapeutic platinum. This study proves the great potential of MNPs for combinational cancer therapy, providing a new insight for the next generation of nanomedicines.

Introduction

Cancers are some of the most challenging and life-threatening diseases for human beings.[1–3] Among them, liver cancer is the fourth most frequent cause of cancer associated death worldwide, with a high rate of recurrence,[4] possibly due to the existence of liver cancer stem cells (CSCs).[5] CSCs, also called tumor initiating stem-like cells, are a subset of cancer cells with progenitor-like properties. They can self-renew and produce heterogeneous progeny, resulting in cancer heterogeneity.[6,7] Mounting evidence has confirmed that CSCs are responsible for cancer metastasis and relapse, with their highly invasive ability to initiate and repopulate tumor tissues as well as their resistance to chemotherapy and radiation.[8] Therefore, it is of importance to develop a therapeutic method to kill CSCs in order to completely eradicate cancers.

Nanotechnology-based cancer therapeutic systems have shown promising results in medical technology, greatly improving the therapeutic performances of many existing drugs and implementing entirely new therapies.[9–12] The nanoparticles developed thus far are able not only to finely tune the pharmacokinetics and tissue distribution of the drugs, but they are also able to combine different therapeutic modalities into one system to achieve a synergetic effect on cancer eradication.[13–17] For example, photodynamic therapy (PDT), a rapidly developing cancer treatment, transforms tissue oxygen into toxic singlet oxygen to kill tumor cells in the presence of light and photosensitizers.[18–20] PDT is an excellent complement to chemotherapy due to its negligible drug resistance, minimal invasion, and non-severe side effects to

[a] *Division of Hepatobiliary and Pancreatic Surgery, Department of Surgery, First Affiliated Hospital, School of Medicine, Zhejiang University, NHFPC Key Laboratory of Combined Multi-organ Transplantation, Key Laboratory of the Diagnosis and Treatment of Organ Transplantation, CAMS, Key Laboratory of Organ Transplantation, Collaborative Innovation Centre for Diagnosis Treatment of Infectious Diseases, Zhejiang Province, Hangzhou, 310003, China. E-mail: shusenzheng@zju.edu.cn*

[b] *MOE Key Laboratory of Macromolecular Synthesis and Functionalization, Department of Polymer Science and Engineering, Zhejiang University, Hangzhou 310027, China. E-mail: zwmao@zju.edu.cn*

[c] *Department of General Medicine, Second Affiliated Hospital of Zhejiang Chinese Medical University, Hangzhou, 310003, China*

[d] *Department of Surgery, The Second Affiliated Hospital and Yuying Children's Hospital of Wenzhou Medical University, School of Medicine, Wenzhou 325027, China*

[e] *Laboratory of Molecular Imaging and Nanomedicine, National Institute of Biomedical Imaging and Bioengineering, National Institutes of Health, Bethesda, Maryland 20892, USA. E-mail: guocan.yu@nih.gov*

† Electronic supplementary information (ESI) available. See DOI: 10.1039/c9tb01299k

‡ These authors contributed equally to this work.

This journal is © The Royal Society of Chemistry 2019

Published on 29 August 2019. Downloaded by Queen Mary, University of London on 3/3/2022 3:14:37 PM.

marginal tissues and other major organs that occur with conventional cancer treatments.[21] In our previous study, we demonstrated that an organoplatinum(II) metallacage is formed *via* multicomponent coordination-driven self-assembly using cytotoxic *cis*-$(PEt_3)_2Pt(OTf)_2$ (cPt), 5,10,15,20-tetra(4-pyridyl)porphyrin (TPP), and disodium terephthalate (DSTP) as the building blocks.[22] Upon formation of the metallacage, the intermolecular π–π stacking of TPP is effectively suppressed, resulting in a significant enhancement of reactive oxygen generation, which is favorable for PDT and combinational photochemotherapy. Then, the hydrophobic metallacage was encapsulated into amphiphilic polymer micelles composed of mPEG-*b*-PEBP and RGD-PEG-*b*-PEBP *via* charge interaction and hydrophobic force; this enabled the metallacage-loaded NPs (MNPs) to exhibit long blood circulation times as well as selective tumor accumulation and internalization *via* the enhanced permeability and retention (EPR) effect and active targeting ability. The MNPs exhibit excellent photochemotherapy performance against orthotopic hepatoma cancer, effectively preventing tumor recurrence and metastasis after a single treatment. The results suggest that photochemotherapy *via* MNPs may also have superior ability to kill liver CSCs, contributing to exciting therapeutic outcomes.

Many markers including CD133, CD44, CD24, CD90, CD13 and epithelial cell adhesion molecule (EpCAM) have been used to identify liver CSCs and further evaluate cell phenotypes and cellular behaviors.[23–27] CD133 is expressed on the cell surface as an epithelial membrane protein; it has been used to identify several CD133 overexpressing human CSCs. For example, based on magnetic affinity cell sorting (MACS), Singh *et al.* separated CD133+ human brain cancer cells; these cells are able to self-renew and recapitulate primary brain cancer at a density of 100 cells per mouse *in vivo*.[28,29] Moreover, increased CD133 expression in Huh7 cells was correlated with tumor initiation, which is regulated by the mechanism between TGF-β signaling and epigenetic modification.[30] Therefore, CD133 can be used as a marker to identify and select CSCs. CD44, which is recognized as an effective marker of CSCs in many cancers,[31,32] can also be used to identify CSCs.

Non-adherent or ultralow attachment based three-dimensional cell culture is a classical and most widely used sorting method to isolate and enrich CSCs, based on self-renewal and anoikis resistance of CSCs.[33] By using the ultralow attachment 3D culture separation method combined with CD133 selection, we identified and isolated CCLP-1 CSCs and Huh7 CSCs with subsequent classical characterization of cancer stem cell properties, such as high sphere formation ability, tumor formation ability in mice, and expression of core transcription factors (including OCT4, Sox2, and NANOG) in CSCs.[34–37]

With the selected two kinds of liver CSCs in hand, in this study, we aim to reveal the photochemo-toxicity of MNPs on the liver CSCs upon light irradiation, and its underlying mechanism, *via* both the classic 2D cell culture model and the 3D cell spheroid model, to further evaluate the translational potential of MNPs in clinical therapy.

Materials and methods

Preparation and characterization of MNPs

The MNPs were fabricated using a co-precipitation method reported before.[19] cPt (29.2 mg, 40 mM), TPP (6.18 mg, 10 mM) and DSTP (4.2 mg, 20 mM) were mixed and heated in an acetone/water mixture (v/v = 4/1) at 70 °C for 4 h to generate discrete metallacages. mPEG-*b*-PEBP (45.0 mg), RGD-PEG-*b*-PEBP (5.0 mg), and metallacages (20.0 mg) were solubilized in acetone (5 mL), and then slowly added into MilliQ water (20 mL) under sonication. After sonication for 10 min, the organic solvent was completely removed under vacuum to obtain the MNP solution. The polymer NP suspension and PNP (NPs containing TPP) suspensions were prepared *via* similar procedures.

Transmittance electron microscopy (TEM, FEI Tecnai12, FEI, Oregon) and dynamic light scattering (DLS, Zetasizer 3000, Malvern, MA) were used to characterize the obtained MNPs. To measure singlet oxygen generation, MNPs (0.5 μM metallacage) were suspended in a solution containing 5.0 μM singlet oxygen sensor green (SOSG) dye. The mixture was then placed in a cuvette and the solution was irradiated at 638 nm (0.5 W cm^{-2}). The fluorescence emission of SOSG, which is excited at 532 nm, was measured using a fluorescence spectrophotometer (Shimadzu UV-3150).

Cell culture

Human hepatocellular carcinoma cell line HuH7 and intrahepatic cancer cell line CCLP-1 were obtained from the Shanghai Institute of Biochemistry and Cell Biology, Chinese Academy of Sciences (Shanghai, China). Huh7 and CCLP-1 cells were maintained in DMEM (Biological Industries, Israel) supplemented with 10% FBS (Moregate Biotech, Australia). Huh7 CSC and CCLP-1 CSCs were cultured in cancer stem cell culture medium (CSCM), which consists of serum-free DMEM-F12 medium (Thermo Fisher, MA, USA) supplemented with basic fibroblast growth factor (bFGF, Peprotech, Rocky Hill, NJ, USA), epidermal growth factor (EGF, Pepro Tech Inc, USA), Leukemia Inhibitory Factor (LIF, Peprotech, USA), and B27 (Thermo Fisher, USA), in ultralow-attachment 6-well plates (Corning, NY, USA). CSCs were passaged with accutase (Yeasen, Shanghai, China) every 5 days. All cells were cultured at 37 °C in an incubator under 5% CO_2.

Magnetic affinity cell sorting (MACS) and separation of liver CSCs

The CD133 MicroBead Kit (Miltenyi Biotec, Germany) was purchased and magnetic affinity cell sorting (MACS) was performed to isolate CD133+ huh7 cells according to the manufacturer's protocols. Huh7 cells were suspended in a single-cell suspension with a cell density of 1.0×10^4 cells per mL. Cells were washed with MACS buffer, and then treated with the microbead-conjugated CD133 antibody. After carefully mixing, cells were incubated at 4 °C for 15 min in the dark. Subsequently, cells were centrifuged at 300*g* for 3 min and were washed with MACS buffer twice. The cells were re-suspended at a density

Published on 29 August 2019. Downloaded by Queen Mary, University of London on 3/3/2022 3:14:37 PM.

of 2×10^4 cells per mL and then transferred into a column in a magnetic field for cell separation. During separation, CD133− cells were first washed off. After removing the column from the magnetic field, 500 μL of MACS buffer was added to elute CD133+ cells from the column. CCLP-1 cells and CD133+ Huh7 cells were cultured in ultralow-attachment 6-well plates, in serum-free DMEM-F12 medium supplemented with cytokines. Culture medium was changed every 4 days and floating spheroids were collected and moved to another well. Every surviving spheroid was digested into single cells by using accutase for the next round of selection. This procedure was repeated three times to harvest huh7 CSCs.

Cytotoxicity study

Cell Counting Kit-8 (CCK-8) assay was performed to evaluate the cytotoxicity. 2.0×10^3 suspended cells per well were seeded onto 96-well plates and cultured for 24 h to allow attachment. Fresh media containing different concentrations of cPt, PNP, PNP + cPt (cPt/PNP = 4 : 1, molar ratio) and MNPs were used to replace the culture medium, respectively. In the rescue assay, NAC (a classical ROS scavenger) was added into the culture medium in the meantime. After an overnight incubation, the groups treated with PNP + L (mono-PDT) and MNP + L (photo-chemotherapy) were irradiated with 638 nm light (0.5 W cm^{-2}, 1 min). The cells were cultured for another 12 h after irradiation. After the supernatant was removed, cells were incubated in a mixture of 10 μL of CCK-8 test solution and 90 μL of serum-free DMEM medium at 37 °C for 1 h. The absorbance was detected using a spectrophotometer (450 nm, BioTek, USA). All experiments were carried out with four replicates. The cells incubated in DMEM containing 10% FBS were used as a control (100%).

Western blotting

CSCs were treated with cPt, PNPs, PNP + cPt (cPt/PNP = 4 : 1, molar ratio), and MNPs at molar concentrations of 50 nM or 100 nM. After 12 h of incubation, the cells in the PNP + L and MNP + L groups were irradiated at 638 nm (0.5 W cm^{-2}, 1 min) and incubated for another 12 h. Cells were collected in RIPA Lysis Buffer (Beyotime Biotechnology, China) and sonicated. Bradford assay (Bio-Rad Laboratories, Inc., Hercules, CA, USA) was used to measure protein concentration. Antibodies recognizing total and cleaved caspase 3 (#9662S), total and cleaved caspase 9 (#9509S), poly ADP-ribose polymerase (PARP, #9532S), Bcl-2 homologous antagonist (BAK, #3814S), and glyceraldehyde-3-phosphate dehydrogenase (GAPDH, #5174S) were obtained from Cell Signaling Technology (Danvers, MA, USA). Western blotting experiments were performed as previously described.[38]

Immunofluorescence

Cells were seeded onto confocal dishes (Thermo Fisher, MA, USA) and incubated overnight for attachment. After different treatment, cells were washed with PBS once and fixed by 4% paraformaldehyde in PBS for 0.5 h at room temperature. Cells were then washed with PBS three times, and treated with 5% BSA blocking buffer for 1 h. After being washed with PBS, cells were treated with the first antibodies (against OCT4, NANOG and Sox2, respectively) in 3% BSA buffer overnight at 4 °C. The cells were incubated with secondary antibodies for 1 h, after washing with PBS three times. After being washed with PBS three times, the cells were further stained with DAPI (4,6-diamino-2-phenylindole), and then observed *via* confocal laser scanning microscopy (CLSM, IX82, Olympus, Japan).

Colony formation assay

Suspended cells were seeded into six-well plates at a density of 1.0×10^3 cells per well in DMEM medium containing 10% FBS and cultured for 2 weeks. After being washed with PBS, cells were fixed by 4% paraformaldehyde in PBS for 15 min and stained with 0.2% crystal violet for 30 minutes. Cells were washed with PBS three times and counted under an optical microscope (IX82, Olympus, Japan). All experiments were performed three times.

Spheroid formation assay

Suspended cells were seeded into ultralow attachment six-well plates (Corning, NY, USA) at a cell density of 1.0×10^3 cells per well in serum-free cancer stem cell culture medium (CSCM) for 2 weeks. The number of spheroids of each group was measured under an optical microscope. The size of spheroids was quantitatively analyzed according to methods reported in the literature.[39] All experiments were performed three times.

Living/dead cell staining

CSCs were seeded into 96-well plates at a density of 3.0×10^4 cells per well and allowed to attach overnight. The cells receiving different treatments (L, cPt, PNP + L, PNP + cPt + L, MNPs and MNP + L) were washed and then stained with 100 μl of PI/FDA mixed solution (including 97.9 μl of PBS, 2 μl of PI solution and 0.1 μl of FDA solution) for 20 minutes at room temperature under darkness. After careful washing with PBS, cells were observed under a fluorescence microscope.

Cell apoptosis assay

CSCs were seeded into ultralow attachment six-well plates at a density of 1.0×10^5 cells per well. After washing with PBS, cells were digested into single cells and again washed with PBS. The cells were then stained by an Annexin V-FITC Apoptosis Detection Kit (BD, NY, USA) according to the manufacturer's protocol. Flow cytometry was performed by using a BD LSR II instrument (BD Biosciences, San Jose, CA, USA). At least 1.0×10^4 cells were analyzed in each experiment and further analyzed.

Cell migration assay

CSCs were seeded into Milli-cell cell culture inserts (24-well plate, 8 μm pore size, Millipore, USA) at a density of 5.0×10^4 cells per well with 200 μL of serum-free DMEM. 800 μL of DMEM containing 10% FBS was added into the bottom chamber. After incubation, CSCs were fixed using 4% paraformaldehyde for 15 min, and then they were stained with

 This journal is © The Royal Society of Chemistry 2019

Published on 29 August 2019. Downloaded by Queen Mary, University of London on 3/3/2022 3:14:37 PM.

0.2% crystal violet for 30 min. After being washed with PBS three times, the migrated cells were counted under a microscope.

Detection of ROS and JC-1 levels

A ROS detection kit and a JC-1 detection kit (Beyotime, Shanghai, China) were used to determine the intracellular ROS level and the integrity of the mitochondrial membrane, respectively. CSCs were seeded in 24-well plates (8.0×10^4 cells per well) and incubated for 12 h. After treatment with different groups (L, cPt, PNP + L, PNP + cPt + L, MNPs and MNP + L), the cells were washed with PBS and then treated with 500 μL of fresh serum-free medium consisting of 10 μM DCFH-DA and incubated for 15 min. After being washed twice with PBS, cells were observed under a fluorescence microscope (Leica, Wetzlar, Hessen, Germany). Another batch of cells was trypsinized and collected for further analysis using flow cytometry.

After different treatments, CSCs were washed with PBS twice and then treated with 500 μL of JC-1 working solution. After 20 min of incubation, cells were washed with cold JC-1 staining buffer. CSCs were observed under a fluorescence microscope or trypsinized for analysis using flow cytometry.

Cytotoxicity study in the cell spheroid model

CSCs were cultured in ultralow attachment 6-well plates with serum-free CSCM to form spheroids; they were then moved to a 96-well plate. After different treatments, spheroids were stained with PI/FDA, and then observed *via* CLSM.

Tumor xenograft experiments

All animal experiments were carried out according to the requirement of the guidelines of the National Institutes of Health (Guide for the Care and Use of Laboratory Animals, 2011). All procedures performed in studies involving animals were in accordance with the ethical standards of the First Affiliated Hospital of Zhejiang University School of Medicine and approved by the ethics committee of Zhejiang University. Healthy male nude mice, 4–6 weeks old, were purchased from the animal center of Zhejiang Academy of Medical Sciences. After treatments, CSCs were digested into single cells and re-suspended at a density of 5.0×10^6 cells per mL. 100 μL of cell suspension was subcutaneously injected into the mice. At determined time points, mice were sacrificed to collect tumors for weighing and recording.

Statistical analysis

Data are reported as mean ± SD. Statistical analysis was performed using the SPSS 22.0 software. The two-tailed Student's *t*-test was used to determine the significance between two groups. One-way ANOVA analysis followed by Tukey's post-test was used to determine the significance of different groups. *: $p < 0.05$, **: $p < 0.01$, ***: $p < 0.001$.

Results

Characterization of metallacage loaded nanoparticles

In our previous study, a chemotherapeutic drug (cPt) and a photosensitizer (TPP) were used as building blocks to construct the metallacage, acting as the vertices and faces. The π–π stacking of TPP is significantly inhibited by the formation of the cage-like structure, which is favourable to increase its fluorescence quantum yield and $^1O_2$ generation quantum yield.[22] Since TPP and the as-prepared metallacages are hydrophobic and not well dispersed in aqueous milieu, an amphiphilic block polymer PEBP-*b*-PEG-RGD was used to encapsulate them into the core of hydrophilic nanoparticles (denoted as PNPs and MNPs, respectively), thereby enhancing their stability in biological media for further *in vitro* and *in vivo* applications. Furthermore, the ingestion of PNPs and MNPs by tumor cells can be expected with the binding ability of RGD moieties to overexpressed integrin on their plasma membrane.

As shown in Fig. 1A, spherical polymer NPs with diameters ranging from 30 to 60 nm were observed in the dry state. A slightly larger hydrophilic diameter was recorded using DLS (Fig. 1B) due to the hydration of the hydrophilic corona of the NPs. An enhancement in diameter was observed after loading TPP or Metallacage into the NP (resulting in PNP or MNP, respectively), indicating the successful encapsulation of cages by the amphiphilic polymers. In addition, the zeta potential of the NP formed by PEBP-*b*-PEG-RGD increased from −48.6 mV to −19.7 mV and −6.2 mV upon encapsulation of TPP and Metallacage, respectively (Fig. 1C), suggesting that the charge–charge interaction is one of the major driving forces in the formation of self-assemblies besides hydrophobic interaction. Solutions containing MNPs in phosphate-buffered saline (PBS) and fetal bovine serum (FBS) at 37 °C were stable for 96 h of incubation and a negligible change in size was found (Fig. S1, ESI†), demonstrating the high colloidal stability of MNPs in biological buffer.

Singlet oxygen sensor green (SOSG) was used to quantify the reactive oxygen species (ROS) generation of nanomaterials upon laser irradiation (638 nm, 0.5 W cm^{-2}). As shown in Fig. 1D, a relatively low fluorescence intensity at 532 nm was observed from PNPs because of the quenching of ROS ascribed to their π–π stacking interactions, even when dispersed with the assistance of amphiphilic polymers. In contrast, the SOSG fluorescence exhibited a significant enhancement upon introduction of metallacage structures (MNPs) under the same conditions, confirming their high photosensitizing efficacy (Fig. 1D). The high yield of ROS generation from MNPs is attributed to the supramolecular cage structure that efficiently prevents the aggregation of TPP molecules, and the incorporation of Pt as heavy atoms into the cage, which is beneficial to convert molecular oxygen to singlet oxygen.[40]

Enrichment and characterization of liver cancer stem cells

CD133 positive cancer cells were recognized as potential cancer initiating cells in liver cancer. Therefore, CD133+ cells were first separated by MACS assay from primary Huh7 cells. For example, as shown in Fig. S2 (ESI†), 88.5% CD133+ Huh7 cells were enriched after selection. In contrast, only 24.2% of Hub7 cells can be identified as CD133+ cells in the control group. After separation, CD133+ Huh-7 cells and CCLP-1 cells were further selected and enriched by continuous culture in a serum-free

Published on 29 August 2019. Downloaded by Queen Mary, University of London on 3/3/2022 3:14:37 PM.

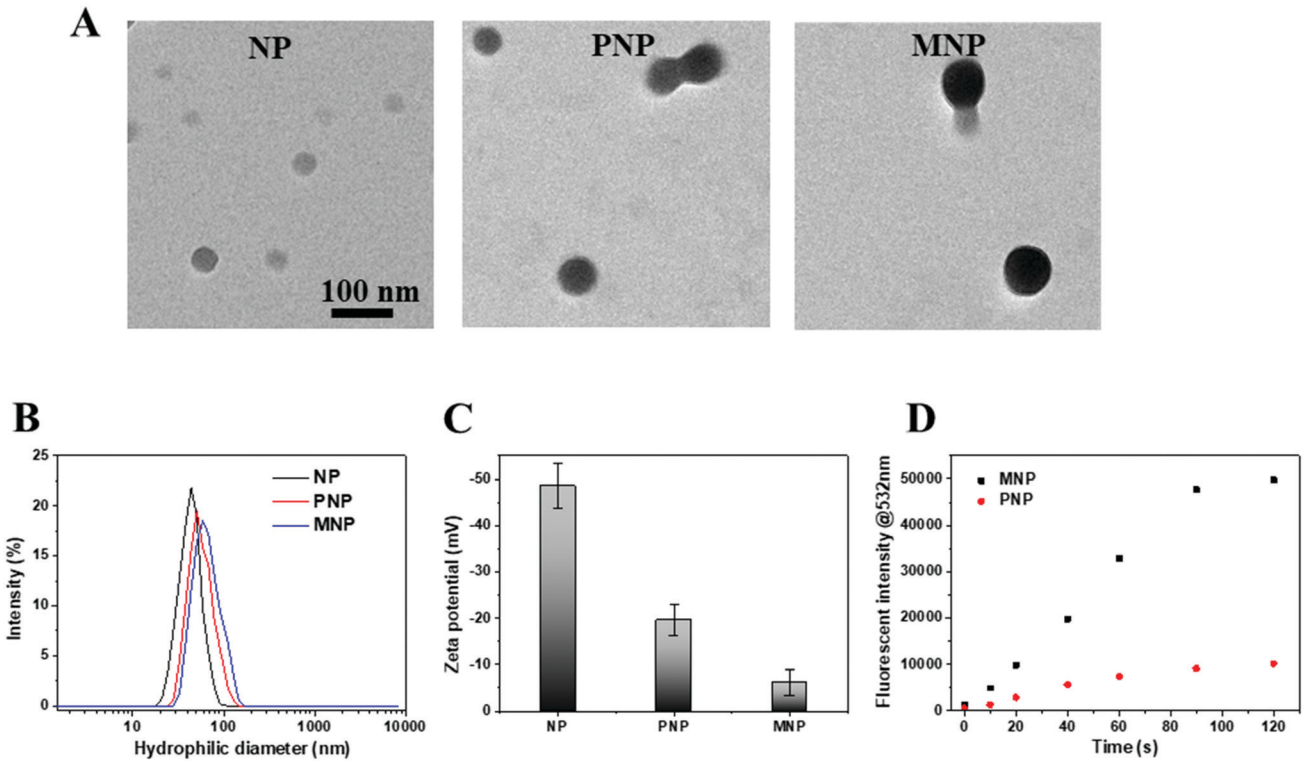

Fig. 1 (A) Representative TEM images, (B) size distribution, and (C) surface zeta potential of NPs, PNPs and MNPs, respectively. (D) Fluorescence intensity of the solution containing SOSG and different nanoparticles at 532 nm as a function of irradiation time (638 nm, 0.5 W cm^{-2}).

and ultra-low attachment system to get Huh-7 CSCs and CCLP-1 CSCs, respectively (Fig. 2A). The expression levels of hall marker genes such as Sox2, Oct4 and Nanog were evaluated to further confirm the stemness of the selected and enriched CSCs.

The expressions of Sox2, OCT4 and NANOG genes were found to be increased significantly in selected and enriched CCLP-1 CSCs and Huh7 CSCs (Fig. 2E and Fig. S2c, ESI†). Both established CCLP-1 CSCs and Huh7 CSCs show stronger spheroid formation ability (Fig. 2B and Fig. S2d, ESI†), and lower clone formation ability (Fig. 2C and Fig. S2e, ESI†), suggesting that both selected and enriched CCLP-1 CSCs and Huh7 CSCs have stronger stemness compared to the original corresponding cancer cells. The xenograft formation experiment also confirmed that CCLP-1 CSCs have a much stronger tumor formation ability *in vivo* (Fig. 2D).

Enhanced synergistic cytotoxicity of MNPs against liver CSCs in a single cell model

Successful cellular uptake of MNPs is one of the key steps for effectively killing cancer stem cells. Cyclo(Arg-Gly-Asp-D-Phe-Lys) (cRGDfK), which could bind to the $\alpha_v\beta_3$ integrin receptor, which is often overexpressed on cancer cells, has been adopted in our design of MNPs for efficient cell uptake. The uptake rate of MNPs by CCLP-1 CSCs was investigated, taking advantage of the auto-fluorescence of MNPs. As shown in Fig. S3 (ESI†), both CCLP-1 normal cancer cells and cancer stem cells showed similar uptake patterns of nanoparticles, possibly due to high integrin expression on both cells.

Cell death of CSCs receiving different treatments was observed after PI/FDA staining. As shown in Fig. S2g (ESI†), on one hand, the MNP + L group has more dead CCLP-1 CSCs (red fluorescence) and less surviving cells (green fluorescence). On the other hand, increasing numbers of dead CCLP-1 CSCs were observed in the MNP + L group, with prolonged irradiation time, *i.e.* from 10 s to 120 s, demonstrating the time-dependent cytotoxicity of MNPs in the presence of laser irradiation. Similar results were observed from Huh7 CSCs (Fig. S4d, ESI†). Since a lower light energy density and shorter irradiation time are preferred for phototherapy, we chose a fixed light irradiation condition (0.5 W cm^{-2}, 1 min) for the following cell experiments.

As shown in Fig. 3A, the survival rate of the CSCs cultured on a traditional 2D surface decreased after receiving different treatment, including cPt, PNP + L, cPt + C+ L, MNP, and MNP + L, in a concentration-dependent manner. The half maximal inhibitory concentration (IC_{50}) of cPt against CCLP-1 CSCs is 1.04 ± 0.24 μM. The IC_{50} value of MNPs in the dark decreased to 0.35 ± 0.09 μM (based on the molar amount of cPt). As for mono-PDT, the IC_{50} value of PNPs was calculated to be 1.72 ± 0.17 μM in the presence of 638 nm light irradiation (0.5 W cm^{-2}, 1 min). The IC_{50} value of the PNP + cPt group upon irradiation was 0.29 ± 0.07 μM, which is lower than that of PNPs (mono-PDT) and cPt (mono-chemotherapy) alone, suggesting that PDT and chemotherapy can achieve a synergistic effect against CCLP-1 CSCs even by simply mixing two therapeutic agents together. The most exciting result is that the IC_{50} value of MNPs

 This journal is © The Royal Society of Chemistry 2019

Published on 29 August 2019. Downloaded by Queen Mary, University of London on 3/3/2022 3:14:37 PM.

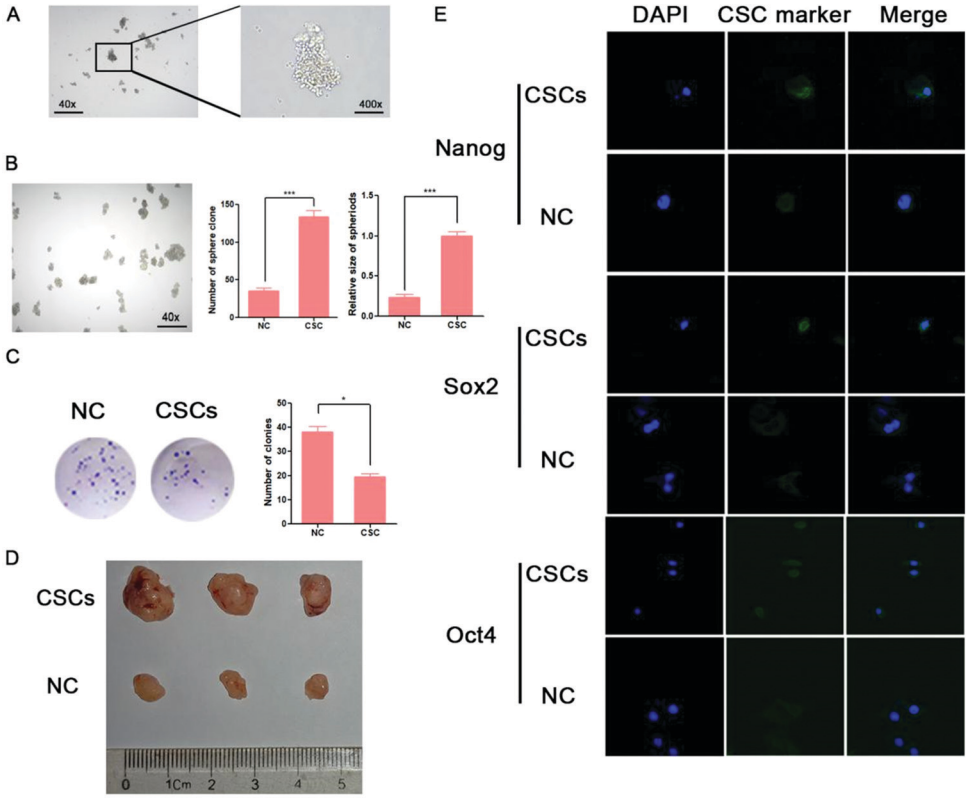

Fig. 2 Selection and characterization of CCLP-1 CSCs. (A) Images of CCLP-1 CSCs derived from the CCLP-1 cancer cell line *via* 3D ultralow-attachment successive cultivation. (B) Spheroid formation, (C) clone formation and (D) tumorigenesis of CCLP-1 cancer cells and CCLP-1 CSCs, respectively. $*P < 0.05$, $***P < 0.001$. (E) Fluorescent imaging of CCLP-1 cancer cells and CCLP-1 CSCs stained with DAPI (blue) and different stem cell markers (green color: Nanog, Sox2 and Oct4, respectively). All the images were amplified by 400 times.

upon irradiation is 0.10 ± 0.33 μM, showing a much more powerful synergic cytotoxicity against CCLP-1 CSCs. The excellent combinational toxicity can be attributed to the complementary toxic mechanisms of PDT and chemotherapy when integrated into one nanoplatform and in turn performed on CSCs simultaneously and precisely at the same location.

Cytotoxicity of MNPs against Huh7 CSCs was assessed as well (Fig. S4a, ESI†). The IC_{50} value of cPt (0.68 ± 0.17 μM), MNPs (0.19 ± 0.07 μM), PNPs (0.38 ± 0.06 μM), cPt + PNP (0.39 ± 0.06 μM), and MNP + L (0.043 ± 0.006 μM) against huh7 CSCs was calculated. The results are similar in trend with those of CCLP-1 CSCs. All these data demonstrate the synergistic effect of chemotherapy and PDT endowing MNPs with enhanced cytotoxicity against liver CSCs upon irradiation.

Furthermore, the migration ability and spheroid formation ability of liver CSCs, which reflect the tumor metastasis and recurrence abilities, were studied after they received different treatments. As shown in Fig. 3C and Fig. S4b (ESI†), the migration ability of CSCs in the MNP + L group reduced significantly, while the mobility of cells in other groups was largely retained. Meanwhile, CCLP-1 CSCs in the MNP + L group exhibited a significant decrease of tumor spheroid number and size *in vitro*, compared with other groups (Fig. 2D). These results support the conclusion that MNP + L has the best efficiency to destroy liver CSCs and prevent their recurrence and metastasis.

Since both PDT and chemotherapy may induce cell apoptosis, the apoptosis stage of CSCs receiving different treatments was further analyzed by PI/Annexin V-FITC staining (Fig. 3B and Fig. S4c, ESI†). For the CCLP-1 CSCs treated with cPt, the subpopulations of the late apoptosis and early apoptosis stages were 5.2% and 9.0%, respectively, which are close to those of MNPs without irradiation (7.6% and 13.9%). When treated with PNP + L, the subpopulations of the early apoptosis and late apoptosis stages were 3.6% and 3.7%, respectively, similar to the trend of cytotoxicity. The subpopulations of the early apoptosis and late apoptosis stages increased to 7.11% and 17.5%, respectively, in the cPt + PNP + L group. Excitingly, the apoptotic rate of CSCs in the MNP + L group significantly increased to 69.3% (16.3% for late apoptosis and 53.0% for early apoptosis), suggesting the highest toxicity of combinational photochemotherapy.

Mechanism of cytotoxicity

In the process of PDT, energy is transferred from a photosensitizer to molecular oxygen upon irradiation, generating reactive oxygen species (ROS) and resulting in oxidative damage of lipids, proteins, and nucleic acids; this ultimately causes death of cancer cells. Therefore, ROS generation is an important step in PDT-induced cell death and needs to be studied. DCFH-DA, a cell membrane permeable fluorescent dye, was used to detect the

Published on 29 August 2019. Downloaded by Queen Mary, University of London on 3/3/2022 3:14:37 PM.

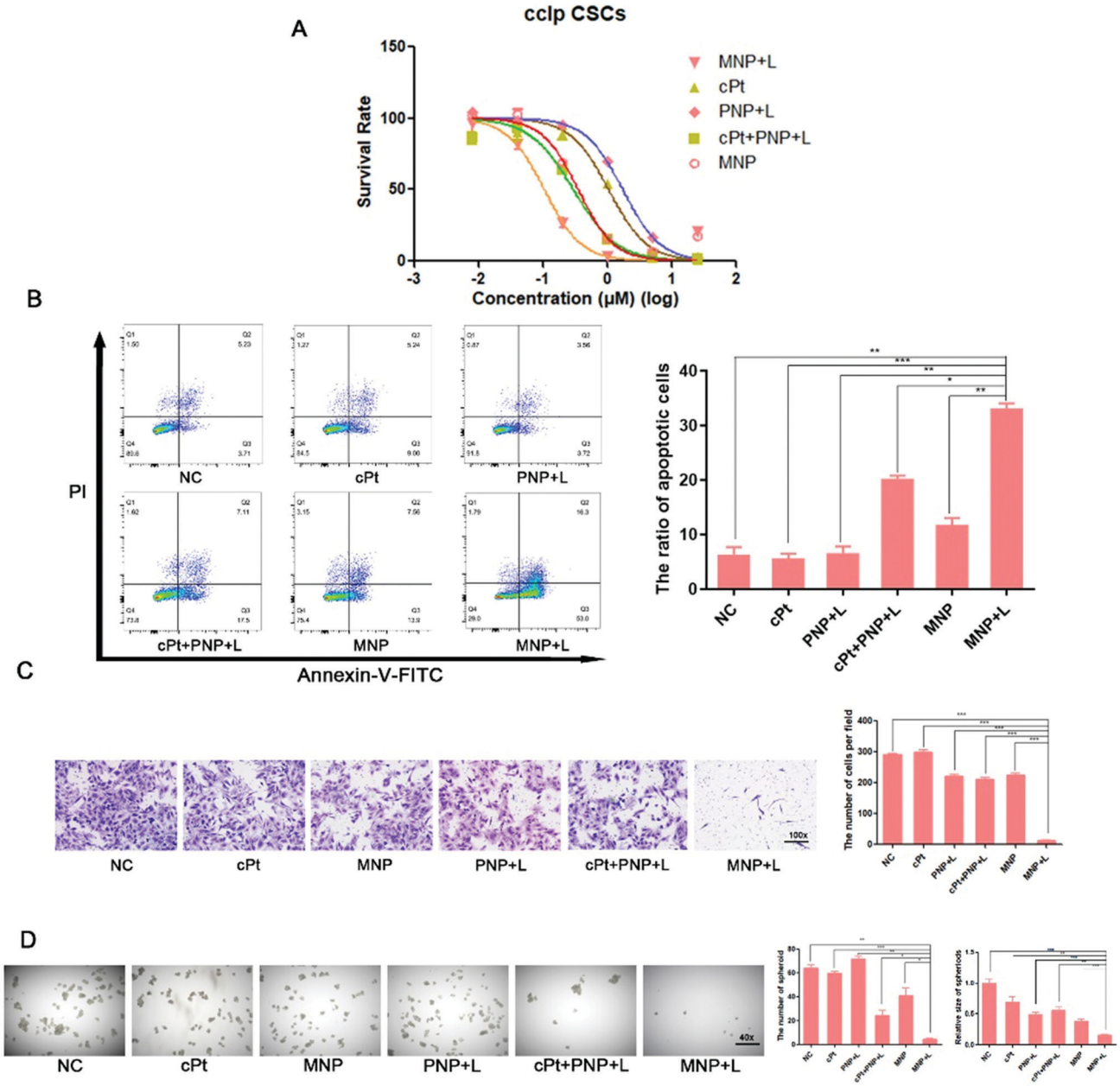

Fig. 3 Cytotoxicity of MNPs against CSCs *in vitro*. (A) Survival rate of CCLP-1 CSCs treated with different groups. The cells in the light irradiation groups were irradiated under 638 nm light (0.5 W cm^{-2}, 1 min). (B) Cell apoptosis, (C) migration and (D) spheroid formation ability of CCLP-1 CSCs receiving different treatments, respectively. The images of migrated cells and generated spheroids were magnified 100 times and 40 times, respectively. $*p < 0.05$, $**p < 0.01$, $***p < 0.001$.

intracellular ROS level. As shown in Fig. 4A, no obvious fluorescent signal was observed from the CCLP-1 CSCs in NC, light only, and cPt groups. The fluorescent signal became slightly stronger from the CSCs in the PNP + L and PNP + cPt + L groups. In contrast, a significant enhancement of fluorescence was detected from the CCLP-1 CSCs in the MNP + L group, indicating the highest ROS level due to the significantly enhanced ROS generation yield in the presence of metallacage structures (Fig. 4B). Similar results were observed from Huh7 CSCs (Fig. S5a and b, ESI†), suggesting the broad anti-cancer effect of our photochemotherapy system. To confirm the ROS generation and induced cell death, NAC, a ROS scavenger, was used to eliminate generated ROS in the MNP + L group. As expected, NAC partly prevented the death of both CSCs induced by MNPs upon irradiation (Fig. 4F and Fig. S5c, ESI†).

It has been verified that excessive ROS lead to mitochondrial apoptosis in cells.[41] Herein, we speculated that MNPs could produce sufficient ROS rapidly upon light irradiation, a situation that leads to mitochondrial injury and cell apoptosis. Therefore, the mitochondrial membrane potential ($Mt\Delta\psi$), which reflects the integrity of mitochondria, was detected using JC-1 assay, where red fluorescence indicated

 This journal is © The Royal Society of Chemistry 2019

Published on 29 August 2019. Downloaded by Queen Mary, University of London on 3/3/2022 3:14:37 PM.

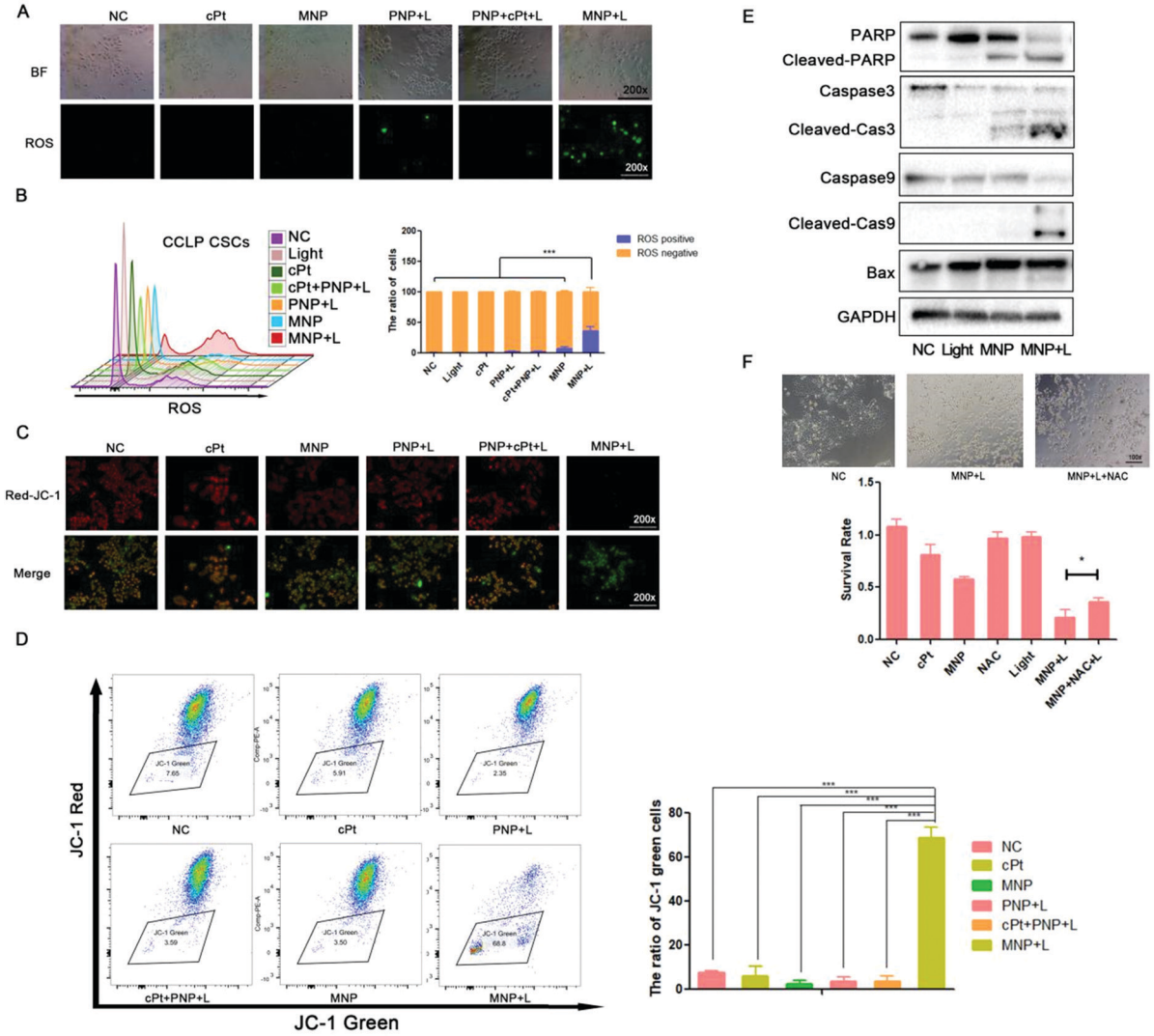

Fig. 4 Detection of ROS production, mitochondrial injury and following cellular apoptosis by MNPs. (A) Fluorescence images and (B) quantitative ROS levels in CCLP-1 CSCs receiving different treatments. (C) Fluorescence images and (D) quantitative determination of mitochondrial membrane integrity in CCLP-1 CSCs receiving different treatments, respectively. The fluorescence images were magnified 200 times. The cells in the light irradiation groups were irradiated under 638 nm light (0.5 W cm^{-2}, 1 min). (E) Western blot analysis of the expressions of apoptosis related proteins. (F) Representative optical images (amplified 100 times) of pristine CCLP-1 CSCs, CSCs treated with MNP + L, and CSCs treated with MNP + L in the presence of NAC. The survival rate of CCLP-1 CSCs was then quantified after different treatments. The light irradiation condition was 0.5 W cm^{-2} for 1 min. *$p < 0.05$, ***$p < 0.001$.

a high Mt$\Delta\psi$, and green fluorescence indicated a low Mt$\Delta\psi$. As shown in Fig. 4C and D, an obvious increase of ratio of green fluorescent positive cells was observed from CCLP-1 CSCs in the MNP + L group, suggesting severe mitochondrial damage induced by photochemotherapy. A similar trend was also observed from the Huh7 CSCs (Fig. S5d, ESI†). In addition, a longer irradiation time leads to stronger green fluorescence from the CSCs in the MNP + L group, indicating more severe mitochondrial injury.

Apoptosis is also characterized by the cleavage of poly(ADP-ribose)polymerase (PARP), which contributes to the catalysis of a variety of nuclear proteins. Such cleavage essentially inactivates the enzyme by destroying its ability to respond to DNA strand breaks. Caspase-3 and caspase-9, two members of the caspase protease family that play a central role in the execution of the apoptotic program, are primarily responsible for the cleavage of PARP during cell death. Therefore, the expression levels of apoptosis associated molecules from the CSCs receiving different treatments, including cleaved-PARP, cleaved caspase-3, cleaved caspase-9 and BAK, were studied using Western blot assay. The results (Fig. 4E) revealed that photochemotherapy (MNP + L) significantly enhanced the expression of proteins associated with the apoptosis pathway, indicating the activation of the apoptosis program. All the results obtained are in favor of our postulation that our nanoplatform is able to destroy CSCs *via* ROS generation, damage of the mitochondrial membrane, and activation of the cell apoptosis pathway.

Published on 29 August 2019. Downloaded by Queen Mary, University of London on 3/3/2022 3:14:37 PM.

Toxicity toward CSCs in tumor spheroids

Accumulating evidence shows that 3D cancer spheroids are more chemo- and radio-therapy resistant, and they are more similar to the natural state of cancer *in situ* than 2D cultured cancer cells.[42] Encouraged by the excellent performance of our nanoplatform against 2D cultured CSCs, we also investigated their anti-cancer performance on CSC multicellular spheroids. As shown in Fig. S5e (ESI†), the integrity of the tumor spheroid was partially destroyed after treatment with photochemotherapy (MNP + L), with noticeable cell debris. In addition, CSCs inside spheroids became swollen or shrank, suggesting that they underwent apoptosis or necrosis processes.

FDA/PI staining was also adopted to distinguish living and dead cells in spheroids. As shown in Fig. 5A and Fig. S5f (ESI†), only a weak red fluorescent signal, which indicates dead cells, was observed from tumor spheroids in cPt, MNP, and PNP + L groups. The results suggested that only CSCs located on the surface of the spheroids can be destroyed by mono-chemotherapy or mono-PDT, which is not enough for eradicating cancer spheroids. In contrast, MNP + L can effectively kill almost all CSCs in spheroids, confirming again the excellent potential of MNPs in cancer treatment in the presence of proper light irradiation. It is worth noting that only a few CSCs were killed in the cPt + PNP + L group, indicating that integration of both chemotherapy and PDT into one nanoplatform is necessary for advanced cancer therapy.

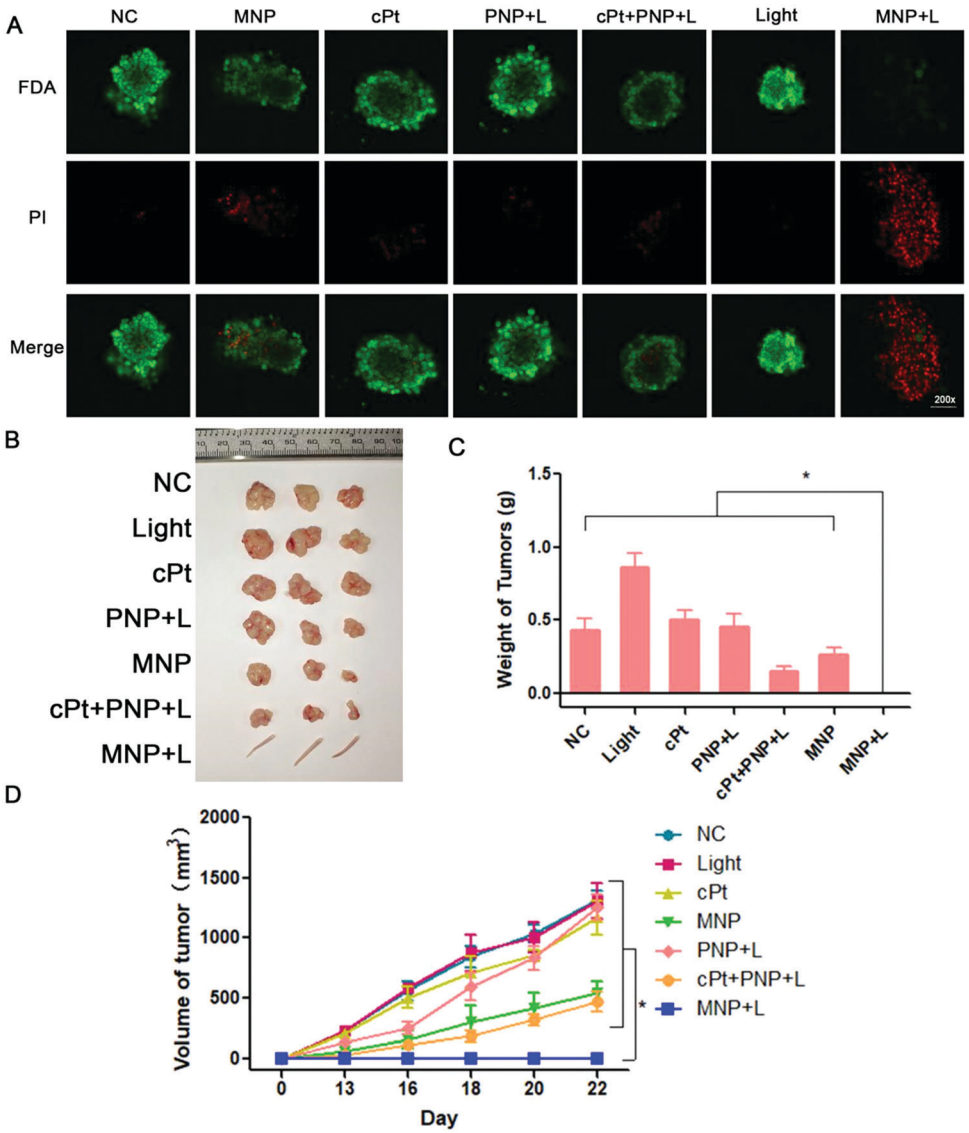

Fig. 5 Cytotoxicity of CCLP-1 CSCs in the spheroid model. (A) CLSM images with a magnification of 200 times of CCLP-1 CSC spheroids receiving different treatments. (B) Optical images and (C) weight, and (D) tumor growth curves of xenograft tumors of CCLP-1 CSCs generated from tumor spheroids receiving various treatments *in vivo*. The CSC spheroids in different groups were irradiated with 638 nm light (0.5 W cm^{-2}, 1 min). Upon treatment, the spheroids were digested into cell suspensions and then transplanted into nude mice to observe tumor formation and growth behaviors (n = 3). * indicates $p < 0.05$. The mouse tail indicates no tumor formation.

 This journal is © The Royal Society of Chemistry 2019

Published on 29 August 2019. Downloaded by Queen Mary, University of London on 3/3/2022 3:14:37 PM.

Featuring high resistance to traditional therapeutic methods, high tumorigenesis ability is another major characteristic of CSCs. In this study, we also tested the tumorigenesis ability of CSCs in the spheroids after different treatments, by subcutaneously injecting the same amount of CSCs into nude mice. As shown in Fig. 5B–D and Fig. S5 (ESI†), CCLP-1 CSCs from the spheroids that received photochemotherapy (MNP + L) had significantly lower tumorigenicity in terms of tumor volume and weight, compared to the other groups. All these results demonstrated the superior ability of MNPs in the presence of light irradiation against CSCs in a spheroid model, indicating that MNPs could provide a powerful nanoplatform for cancer therapy.

Discussion

Many of the current cancer therapy strategies, from classic chemotherapy to radiotherapy, aim to eliminate cancer cells. However, it is known that CSCs or other cells with chemotherapy- or radiation-resistant properties can survive from the first strike and are subsequently capable of regenerating the disease. Therefore, it is of importance to evaluate newly developed therapeutic nanosystems on CSCs, to get a more thorough picture of the translational potential of these systems. In our previous study, a sophisticated porphyrin-based metallacage was prepared through multicomponent coordination-driven self-assembly, and then a multifunctional theranostic platform was generated *via* encapsulation of the metallacage into amphiphilic micelles. The obtained nanosystem exhibited long blood circulation and high tumor accumulation, and possessed a superior ability to ablate several kinds of orthopedic and metastasis tumors by taking advantage of combinational chemotherapy and PDT. Encouraged by these results, we were eager to see if our system can work on CSCs.

In our current study, two kinds of liver CSCs were selected, enriched, and established *via* standard sequential processes including cytokine based magnetic affinity cell sorting and ultralow attachment based three-dimensional cell culture. The stemness was then verified in terms of elevated expression levels of hall marker genes (Sox2, OCT4 and NANOG), stronger spheroid formation ability *in vitro*, and higher tumor xenograft formation ability *in vivo*.

Due to the presence of cRGD molecules on MNPs, they can be efficiently ingested by CCLP-1 CSCs, with a similar rate to the that by CCLP-1 normal cancer cells. The combination of chemotherapy and PDT achieved by MNP + L in the presence of light irradiation displayed superior synergistic efficacy against both CCLP-1 and Huh7 CSCs *in vitro*, evidenced by the significantly lower IC_{50}. More interestingly, the cytotoxicity of MNP + L is stronger than that of PNP + cPt + L on both CSCs, due to the superior ROS generation ability of the cage-like supramolecular structure.

Besides the high cytotoxicity induced by MNP + L, the migration ability and clone formation ability of the CSCs were also significantly impaired. The results suggested that our nanosystem has the potential not only to kill CSCs but also to prevent repopulation of residual cells and their migration to other sites. Even more interestingly, the excellent synergistic therapy outcome of our multifunctional nanosystem is also proved by the ablation of CSCs inside spheroids without subsequent tumor-forming ability, whereas the single therapeutic modality can only kill cells on the surface of spheroids and cannot prevent tumor recurrence after implantation into mice. This merit can be attributed to the interplay of the following factors: (1) the small particle size and high stability of MNPs, which make them feasible for deep tumor penetration; (2) the relatively high cell uptake by the CSCs; (3) the high toxicity of MNPs under light irradiation.

In order to understand the toxicity mechanism of our nanosystem on a cellular and a molecular level, cell apoptosis behavior upon synergistic therapy, and expressions of key proteins in related pathways were then studied. The results suggested that our nanosystem has superior therapeutic ability against CSCs due to high ROS generation, damage of the

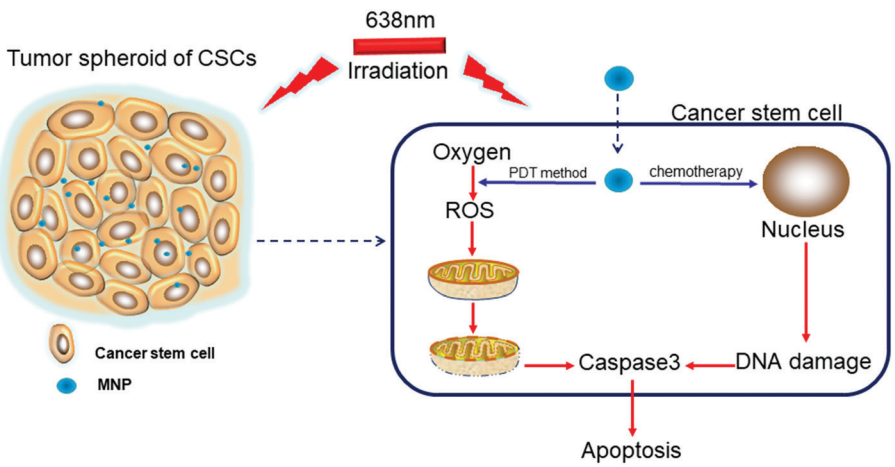

Fig. 6 A scheme summarizing the photochemo-toxicity induced by MNPs in 3D liver CSC spheroids and its potential pathway. MNPs induced ROS generation, injury of mitochondria, and DNA damage in the presence of proper light irradiation, resulting in apoptosis of CSCs.

Published on 29 August 2019. Downloaded by Queen Mary, University of London on 3/3/2022 3:14:37 PM.

mitochondrial membrane and integrity, and activation of the caspase-related cell apoptosis pathway. The mechanistic study provides in-depth understanding of the biological performance of our nanosystem (Fig. 6).

Conclusions

In this study, metallacage-based MNPs with combinational chemotherapy and PDT potential were prepared. The MNPs demonstrate superior therapeutic performance against CCLP-1 and Huh7 liver cancer stem cells in a traditional 2D culture model, inhibiting their viability, mobility, and sphenoid formation ability in the presence of proper light irradiation. Even more importantly, the MNPs can also ablate CSCs inside 3D multicellular spheroids, preventing subsequent tumor formation *in vivo*. MNPs under NIR light irradiation can generate a high level of ROS, leading to damage of the mitochondrial membrane and subsequent cell apoptosis together with chemotherapeutic platinum. This study proves the great synergistic therapeutic potential of MNPs against cancer stem cells, providing a promising strategy for efficient cancer treatment.

Author contributions

B. Y., G. Y., Z. M. and S. Z. conceived and designed the experiments. B. Y., H. L., H. Y., W. C., J. W., X. F., R. T., H. Y., Y. C., Z. L., W. S., B. H., and J. W. performed the experiments and analyzed the data. B. Y., G. Y., Z. M. and S. Z. co-wrote the paper.

Conflicts of interest

There are no conflicts to declare.

Acknowledgements

This study was supported by the Innovative Research Groups of the National Natural Science Foundation of China (No. 81721091 and 51822306), the Major program of the National Natural Science Foundation of China (No. 91542205), the National S&T Major Project (No. 2017ZX10203205), the National Health and Family Planning Commission of China (No. 20161388643), the Science and Technology Department of Zhejiang Province (No. 2015C03034), the Zhejiang Provincial Natural Science Foundation (No. LQ15H160002 and LQ18H160011), the Zhejiang International Science and Technology Cooperation Project (No. 2016C04003), and the General Project Plan of Zhejiang Medical Technology (No. 2016148875).

References

1 B. A. Chabner and T. G. Roberts, *Nat. Rev. Cancer*, 2005, **5**, 65–72.
2 S. Mura, J. Nicolas and P. Couvreur, *Nat. Mater.*, 2013, **12**, 991–1003.
3 J. Shi, P. W. Kantoff, R. Wooster and O. C. Farokhzad, *Nat. Rev. Cancer*, 2017, **17**, 20–37.
4 R. L. Siegel, K. D. Miller and A. Jemal, *Ca-Cancer J. Clin.*, 2019, **69**, 7–34.
5 M. Shackleton, E. Quintana, E. R. Fearon and S. J. Morrison, *Cell*, 2009, **138**, 822–829.
6 C. T. Jordan, M. L. Guzman and M. Noble, *N. Engl. J. Med.*, 2006, **355**, 1253–1261.
7 M. S. Wicha, S. Liu and G. Dontu, *Cancer Res.*, 2006, **66**, 1883–1890.
8 J. A. Magee, E. Piskounova and S. J. Morrison, *Cancer Cell*, 2012, **21**, 283–296.
9 R. A. Petros and J. M. Desimone, *Nat. Rev. Drug Discovery*, 2010, **9**, 615–627.
10 V. P. Torchilin, *Nat. Rev. Drug Discovery*, 2014, **13**, 813–827.
11 B. Xiao, X. Si, M. K. Han, E. Viennois, M. Zhang and D. Merlin, *J. Mater. Chem. B*, 2015, **3**, 7724–7733.
12 A. L. Volsi, D. J. De Aberasturi, M. Henriksenlacey, G. Giammona, M. Licciardi and L. M. Lizmarzan, *J. Mater. Chem. B*, 2016, **4**, 1150–1155.
13 X. Li, X. Zhao, D. Pardhi, Q. Wu, Y. Zheng, H. Zhu and Z. Mao, *Acta Biomater.*, 2018, **74**, 374–384.
14 B. Wang, W. Lin, Z. Mao and C. Gao, *J. Mater. Chem. B*, 2018, **6**, 3145–3155.
15 G. Yu, J. Yang, X. Fu, Z. Wang, L. Shao, Z. Mao, Y. Liu, Z. Yang, F. Zhang and W. Fan, *Mater. Horiz.*, 2018, **5**, 429–435.
16 G. Yu, Z. Yang, X. Fu, B. C. Yung, J. Yang, Z. Mao, L. Shao, B. Hua, Y. Liu and F. Zhang, *Nat. Commun.*, 2018, **9**, 766.
17 G. Yu, B. C. Yung, Z. Zhou, Z. Mao and X. Chen, *ACS Nano*, 2017, **12**, 7–12.
18 J. P. Celli, B. Q. Spring, I. Rizvi, C. L. Evans, K. S. Samkoe, S. Verma, B. W. Pogue and T. Hasan, *Chem. Rev.*, 2010, **110**, 2795–2838.
19 Y. Li, T. Y. Lin, Y. Luo, Q. Liu, W. Xiao, W. T. Guo, D. Lac, H. Zhang, C. Feng and S. Wachsmannhogiu, *Nat. Commun.*, 2014, **5**, 4712.
20 J. F. Lovell, C. S. Jin, E. Huynh, H. Jin, C. Kim, J. L. Rubinstein, W. C. W. Chan, W. Cao, L. V. Wang and G. Zheng, *Nat. Mater.*, 2011, **10**, 324–332.
21 M. Dickerson, B. S. Howerton, Y. Bae and E. C. Glazer, *J. Mater. Chem. B*, 2016, **4**, 394–408.
22 G. Yu, S. Yu, M. L. Saha, J. Zhou, T. R. Cook, B. C. Yung, J. Chen, Z. Mao, F. Zhang and Z. Zhou, *Nat. Commun.*, 2018, **9**, 4335.
23 N. Haraguchi, H. Ishii, K. Mimori, F. Tanaka, M. Ohkuma, H. M. Kim, H. Akita, D. Takiuchi, H. Hatano and H. Nagano, *J. Clin. Invest.*, 2010, **120**, 3326–3339.
24 T. K. Lee, A. Castilho, V. C. H. Cheung, K. H. Tang, S. Ma and I. O. Ng, *Cell Stem Cell*, 2011, **9**, 50–63.
25 S. Ma, W. C. Kwok, T. K. Lee, H. T. Kwan, J. Y. H. Wo, B. Zheng and X. Y. Guan, *Mol. Cancer Res.*, 2008, **6**, 1146–1153.
26 T. Yamashita, J. Ji, A. Budhu, M. Forgues, W. Yang, H. Y. Wang, H. Jia, Q. Ye, L. X. Qin and E. Wauthier, *Gastroenterology*, 2009, **136**, 1012–1024.

 This journal is © The Royal Society of Chemistry 2019

Published on 29 August 2019. Downloaded by Queen Mary, University of London on 3/3/2022 3:14:37 PM.

27 Z. F. Yang, D. W. Ho, M. N. Ng, C. K. Lau, W. C. Yu, P. Ngai, P. Chu, C. T. Lam, R. T. P. Poon and S. T. Fan, *Cancer Cell*, 2008, **13**, 153–166.
28 S. K. Singh, I. Clarke, M. Terasaki, V. E. Bonn, C. Hawkins, J. A. Squire and P. B. Dirks, *Cancer Res.*, 2003, **63**, 5821–5828.
29 S. K. Singh, C. Hawkins, I. D. Clarke, J. A. Squire, J. Bayani, T. Hide, R. M. Henkelman, M. D. Cusimano and P. B. Dirks, *Nature*, 2004, **432**, 396–401.
30 H. You, W. Ding and C. B. Rountree, *Hepatology*, 2010, **51**, 1635–1644.
31 M. Alhajj, M. S. Wicha, A. Benitohernandez, S. J. Morrison and M. F. Clarke, *Proc. Natl. Acad. Sci. U. S. A.*, 2003, **100**, 3983–3988.
32 X. Yang, Y. Xu, B. Yu, J. Zhou, S. Qiu, G. Shi, B. Zhang, W. Wu, Y. Shi and B. Wu, *Gut*, 2010, **59**, 953–962.
33 K. Ishizawa, Z. A. Rasheed, R. Karisch, Q. Wang, J. Kowalski, E. Susky, K. Pereira, C. Karamboulas, N. Moghal, N. V. Rajeshkumar, M. Hidalgo, M. Tsao, L. Ailles, T. K. Waddell, A. Maitra, B. G. Neel and W. Matsui, *Cell Stem Cell*, 2010, **7**, 279–282.
34 O. B. Catherine Adell, K. Antonija and C. H. M. Jamieson, *Clin. Cancer Res.*, 2010, **16**, 3113.
35 J. Duan, W. Qiu, S. Xu, B. Wang, X. Ye, Y. Ping, X. Zhang, X. Bian and S. Yu, *Stem Cells Dev.*, 2013, **22**, 2221–2239.
36 A. Kreso and J. Dick, *Cell Stem Cell*, 2014, **14**, 275–291.
37 V. Tirino, V. Desiderio, F. Paino, A. D. Rosa, F. Papaccio, M. L. Noce, L. Laino, F. D. Francesco and G. Papaccio, *FASEB J.*, 2013, **27**, 13–24.
38 B. Yang, R. Tong, H. Liu, J. Wu, D. Chen, Z. Xue, C. Ding, L. Zhou, H. Xie and S. Zheng, *Int. J. Oncol.*, 2018, **52**, 1235–1245.
39 D. Cassano, M. Santi, F. D'Autilia, A. K. Mapanao, S. Luin and V. Voliani, *Mater. Horiz.*, 2019, **6**, 531–537.
40 Z. Guo, Y. Zou, H. He, J. Rao, S. Ji, X. Cui, H. Ke, Y. Deng, H. Yang, C. Chen, Y. Zhao and H. Chen, *Adv. Mater.*, 2016, **28**, 10155–10164.
41 P. H. Liao, H. Hsu, T. S. Chen, M. C. Chen, C. H. Day, C. C. Tu, Y. Lin, F. J. Tsai, W. Kuo and C. Y. Huang, *Oncogene*, 2017, **36**, 1978–1990.
42 Y. Torisawa, A. Takagi, H. Shiku, T. Yasukawa and T. Matsue, *Oncol. Rep.*, 2005, **13**, 1107–1112.